Kelvin–Helmholtz instability in an ultrathin air film causes drop splashing on smooth surfaces

Yuan Liu[a], Peng Tan[a,b,1], and Lei Xu[a,1]

[a]Department of Physics, The Chinese University of Hong Kong, Hong Kong, China; and [b]State Key Laboratory of Surface Physics, Department of Physics, Fudan University, Shanghai 200433, China

Edited by Wendy Zhang, University of Chicago, Chicago, IL, and accepted by the Editorial Board January 31, 2015 (received for review September 13, 2014)

When a fast-moving drop impacts onto a smooth substrate, splashing will be produced at the edge of the expanding liquid sheet. This ubiquitous phenomenon lacks a fundamental understanding. Combining experiment with model, we illustrate that the ultrathin air film trapped under the expanding liquid front triggers splashing. Because this film is thinner than the mean free path of air molecules, the interior airflow transfers momentum with an unusually high velocity comparable to the speed of sound and generates a stress 10 times stronger than the airflow in common situations. Such a large stress initiates Kelvin–Helmholtz instabilities at small length scales and effectively produces splashing. Our model agrees quantitatively with experimental verifications and brings a fundamental understanding to the ubiquitous phenomenon of drop splashing on smooth surfaces.

drop impact | splash | thin air film | Kelvin–Helmholtz instability

The common phenomenon of drop splashing on smooth surfaces may seem simple and natural to most people; however, its understanding is surprisingly lacking. Splashing is crucial in many important fields, such as the sprinkler irrigation and pesticide application in agriculture, ink-jet printing and plasma spraying in printing and coating industries, and spray cooling in various cooling systems; therefore its better understanding and effective control may make a far-reaching impact on our daily life. Starting in the 19th century, extensive studies on drop impact and splashing have covered a wide range of control parameters, including the impact velocity, drop size, surface tension, viscosity, and substrate properties (1–12), and various splashing criteria have been proposed and debated (13–18). Nevertheless, at the most fundamental level the generation mechanism of splashing remains a big mystery.

Recently a breakthrough has surprisingly revealed the importance of surrounding air and suggested the interaction between air and liquid as the origin of splashing (15, 19, 20). However, this interaction is highly complex: Below the drop air is trapped at both the impact center and the expanding front (21–34), and above it the atmosphere constantly interacts with its top surface. As a result, even the very basic question of which part of air plays the essential role is completely unknown. Moreover, the analysis from classical aerodynamics (18) indicates that the viscous effect from air totally dominates any pressure influence, whereas the experiment contradictorily revealed a strong pressure dependence (15). Even more puzzling, it was revealed that the speed of sound in air plays an important role in splashing generation (15), although the impact speed is typically 10–100 times slower! Therefore, an entirely new and nonclassical interaction, which can directly connect these two distinct timescales, is required to solve this puzzle. Due to the poor understanding of underlying interaction, the fundamental instability that produces splashing is unclear: The prevailing model of Rayleigh–Taylor (RT) instability (35) contradicts the pressure-dependent observation (15, 19, 20), whereas the recent proposition of Kelvin–Helmholtz (KH) instability lacks direct verification (19, 36). Therefore, clarifying the underlying air–liquid interaction and further illustrating the splash-generating instability are currently the most critical issues in the field.

To tackle these issues, we fabricate special porous substrates that enable effective air drainage at carefully designed locations and systematically probe the air–liquid interaction and the splash-generating instability. By making pores at either the impact center or the expanding edge, we reveal that the air trapped under the expanding edge triggers splashing. Because the trapped air is thinner than the mean free path of air molecules, the interior airflow transfers momentum with an unusually high velocity comparable to the speed of sound and generates a stress 10 times stronger than that of the common airflow. Such a large stress initiates Kelvin–Helmholtz instabilities at very small length scales and effectively produces splash. Our model agrees quantitatively with experimental verifications and brings a fundamental understanding to the ubiquitous phenomenon of drop splashing on smooth surfaces.

Results

We release millimeter-sized liquid drops from various heights and impact them onto different substrates. To guarantee reproducible and pronounced splash, we choose liquids with low surface tensions. The liquids are also in the low-viscosity regime where surface tension dominates the viscous effect (19, 20). Three types of substrates are used: smooth substrates, patterned leaking substrates, and patterned nonleaking substrates, as shown in Fig. 1*A*. For patterned substrates made by optical lithography, the diameter of pores is 75 ± 5 μm, much smaller than that of the millimeter-sized liquid drops. The leaking and nonleaking substrates have identical patterns of pores, except

Significance

Liquid drops always splash when they impact smooth surfaces with high enough speeds. This common phenomenon is crucial in many important fields such as agriculture, printing, surface coating, and spray cooling. However, despite extensive studies over one century, the origin of splashing remains a big mystery. Combining experiment with model, we show that the air trapped under the liquid drop forms a special flow within a nanoscale gap. This airflow produces a stress 10 times stronger than the common airflow and generates small Kelvin–Helmholtz instabilities that trigger splash. Our model agrees quantitatively with the experimental verifications and brings a fundamental understanding to the general phenomenon of drop splashing on smooth surfaces.

Author contributions: L.X. designed research; Y.L. and P.T. designed the experiment; Y.L. performed research; Y.L., P.T., and L.X. analyzed data; Y.L., P.T., and L.X. wrote the paper; and L.X. developed the model and supervised the project.

The authors declare no conflict of interest.

This article is a PNAS Direct Submission. W.Z. is a guest editor invited by the Editorial Board.

[1]To whom correspondence may be addressed. Email: xulei@phy.cuhk.edu.hk or tanpeng@fudan.edu.cn.

This article contains supporting information online at www.pnas.org/lookup/suppl/doi:10.1073/pnas.1417718112/-/DCSupplemental.

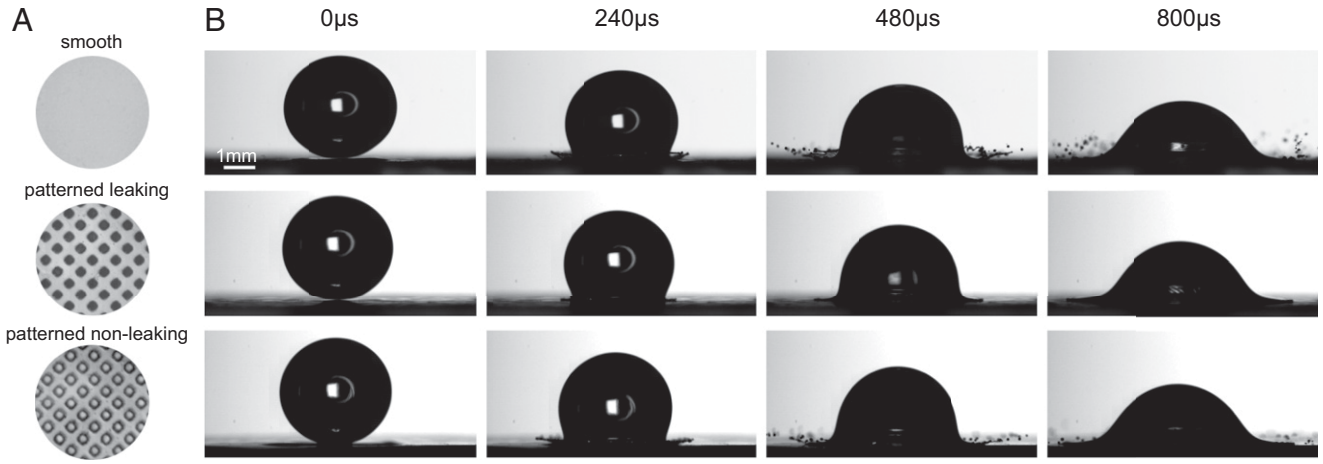

Fig. 1. Distinct splashing outcomes for liquid drops impacting on different substrates. (*A*) Images of the three different substrates: smooth, patterned leaking, and patterned nonleaking substrates. The pore diameter and the spacing between pores are both 75 ± 5 μm. The leaking and nonleaking substrates have identical patterns of pores, except that for the former substrate pores are all of the way through whereas for the latter one they are only halfway through. (*B*) Corresponding splash outcomes for the three types of substrates, for an ethanol drop with diameter 3.5 ± 0.1 mm and impact velocity $V_0 = 1.92 \pm 0.01$ m/s. Splashing occurs significantly on the smooth substrate, disappears completely on the patterned leaking substrate, and reappears on the patterned nonleaking substrate. It clearly demonstrates that the air entrapment under the drop causes splashing.

that for the former case pores are all of the way through whereas for the latter case pores are only halfway through. Thus, the leaking substrate reveals the outcome for impacts with effective air drainage, whereas the nonleaking substrate provides the zero-leakage comparison. All experiments are performed under the atmospheric pressure $P_0 = 101$ kPa and recorded by high-speed photography. To make sure that our results are generally valid, we perform experiments with six different liquids, two different substrate materials, and various impact velocities (*SI Text*). All experiments exhibit consistent behaviors that demonstrate the robustness of our finding.

In Fig. 1*B* we show the corresponding impact outcomes for the three substrates shown in Fig. 1*A*, at the same impact velocity $V_0 = 1.92 \pm 0.01$ m/s (Movie S1). Apparently, splashing occurs significantly on the smooth substrate, disappears on the patterned leaking substrate, and reappears on the patterned nonleaking substrate (Fig. 1 *A* and *B*, *Top*, *Middle*, and *Bottom*, respectively). The complete disappearance of splashing on the leaking substrate unambiguously proves that the air trapped under the liquid causes splashing, and when it drains away splashing vanishes. Furthermore, the reappearance of splashing in the third row of patterned but nonleaking substrate confirms once again that it is air instead of the surface pattern that changes the splashing outcome.

More specifically, air is trapped under the liquid at two distinct locations: the impact center (21–32) and the expanding edge (33) that are separated by a large wetted region in between (Fig. 2*C*). Which entrapment is essential for splashing? We tackle this question with impact experiments on two corresponding substrates as shown in Fig. 2*A*: The top substrate enables a complete drainage of air entrapment at the impact center, whereas the bottom substrate eliminates air entrapment only at the edge. Great care is taken to make sure that the initial contact always occurs at the substrate center. The impact results are demonstrated in Fig. 2*B* (Movie S2): Apparently draining air at the center does not eliminate splashing (Fig. 2*B*, *Top*), whereas removing air entrapment at the edge eliminates splashing completely (Fig. 2*B*, *Bottom*). This finding clearly indicates that it is the air trapped under the expanding edge (33) that plays the essential role.

By making pores at different regions, we clarify that splashing is created by the air entrapment under the expanding front. Next we illustrate the detailed air–liquid interaction within this trapped air. According to the previous experiment (33), this entrapment is an ultrathin air film with a typical thickness of $10 \sim 100$ nm, less than or comparable to the mean free path of air molecules (about 70 nm at $P_0 = 101$ kPa). As a result, the continuous aerodynamics break down and the microscopic picture in the Knudsen regime must be considered. Inside this film, the air molecules right below the liquid surface naturally obtain an average velocity identical to the expanding liquid front, V_e, and then transfer this momentum to the nearby solid surface $10 \sim 100$ nm away (relevant geometry and quantities are shown in Fig. 2 *C* and *D*). Because the travel distance is smaller or comparable to the mean free path, the air molecules essentially reach the solid surface with ballistic motions, which have velocity comparable to the speed of sound. Such a fast motion enables a surprisingly high efficiency in momentum transfer and produces a large stress involving the speed of sound. A detailed calculation by P. G. de Gennes gives the exact expression of the stress (37): $\Sigma_G = \rho_a \cdot c \cdot V_e / \sqrt{2\pi\gamma}$, with ρ_a the density of air (the value at P_0 is used because this air entrainment is directly open to the outside atmosphere as shown in Fig. 2*D*), c the speed of sound in air, V_e the expanding velocity of the liquid front, and $\gamma = 1.4$ the adiabatic gas constant. Therefore, the expression of Σ_G based on the ballistic motion of air molecules in the ultrathin air film naturally connects the two distinct velocities, the speed of sound and the expanding velocity, and explains the outstanding puzzle previously observed (15).

We further illustrate Σ_G by comparing it with the Bernoulli stress from a wind blowing across a liquid surface under common circumstances. For the common airflow, the stress takes the Bernoulli expression of $\rho_a \cdot V_e^2$, which differs from $\Sigma_G \sim \rho_a \cdot c \cdot V_e$ by a typical factor of c/V_e. Plugging in the characteristic values of $c \sim 100$ m/s and $V_e \sim 10$ m/s, clearly Σ_G is larger than the common situation by one order of magnitude and thus behaves as a special airflow 10 times stronger. We propose that this special airflow can initiate KH instabilities around the liquid tip and produce splashing, as schematized in Fig. 2*D* (the dashed curve indicates the instability, drawn not to scale).

To obtain a quantitative understanding, we construct a KH-instability model inside the ultrathin air film. Following the classical work by John W. Miles (38), we write the differential equation for the interface according to stress balance:

$$L\eta + m\frac{d^2\eta}{dt^2} = -p_a. \quad [1]$$

Here $\eta = ae^{i(kx-\omega t)}$ is the small-amplitude disturbance at the interface, L is a linear operator such that $L\eta$ gives the stress resisting a deformation η of the surface, $m = \rho_l/k$ is the effective liquid mass per unit area with ρ_l the liquid density and k the wavenumber, and p_a is the aerodynamic stress acting on the interface. Apparently this equation is equivalent to Newton's second law for a point mass and thus should be generally valid. For a length scale much smaller than the capillary length (~ 1 mm), the gravity can be completely neglected and only surface tension matters, which leads to $L\eta = \sigma k^2\eta$, with σ being the surface tension coefficient of the liquid (38, 39). In particular, the aerodynamic stress can be expressed as $p_a = -\Sigma_G k\eta$, where we have replaced the Bernoulli stress in the original literature with Σ_G and the minus sign corresponds to the KH instability (38).

Plugging in all these terms to Eq. **1** leads to the dispersion relation

$$\omega^2 = \frac{(\sigma k^3 - \Sigma_G k^2)}{\rho_l}. \quad [2]$$

Note that the dispersion relation is time dependent because $\Sigma_G \propto V_e$ varies with time. The system will go unstable once the right-hand side becomes negative, which happens when the destabilizing stress Σ_G overcomes the stabilizing effect from σ. By taking $d\omega/dk = 0$, we obtain the wavenumber of the most dangerous mode that grows the fastest, $k_m = 2\Sigma_G/3\sigma$. Plugging k_m back into Eq. **2**, we get $\omega_m^2 = -(4\Sigma_G^3/27\sigma^2\rho_l)$ and thus the growth rate of the most dangerous mode is $|\omega_m| = \sqrt{4\Sigma_G^3/27\sigma^2\rho_l}$. With typical values from experiment, we can estimate the numerical values of the length scales and timescales for the most dangerous mode: $k_m^{-1} \sim 30$ μm and $|\omega_m^{-1}| \sim 50$ μs. Both values are much smaller than the conventional KH-instability situations. $k_m^{-1} \sim 30$ μm also agrees well with the size of secondary splashing droplets.

Due to the unusually large stress of Σ_G, which is 10 times stronger than the conventional Bernoulli expression, the airflow in an ultrathin air film can generate KH instabilities with an unusually small length scale, $k_m^{-1} = 3\sigma/2\Sigma_G$. The underlying physics are rather straightforward: A gentle breeze can generate slowly varying long-wavelength disturbances, whereas a strong wind may produce much smaller agitations; the exact size depends on the stress balance between the aerodynamic stress, Σ_G, and the restoring response of the interface, the surface tension σ. Because k_m^{-1} is small, tiny undulations that cannot be generated by a regular airflow may now appear.

More interestingly, there is another intrinsic length scale in this problem: the thickness of the liquid sheet, d. Thus, at a specific moment, the instability size k_m^{-1} may match the thickness d and generate a spatial "resonance" in length scales. We propose that it is this spatial resonance that significantly boosts the growth of the instability and causes splashing, as illustrated in Fig. 2*D*. By contrast, on a leaking substrate the ultrathin air film does not exist due to the drainage of air, which consequently eliminates the small KH instability and the splashing, as demonstrated in Fig. 2*E*.

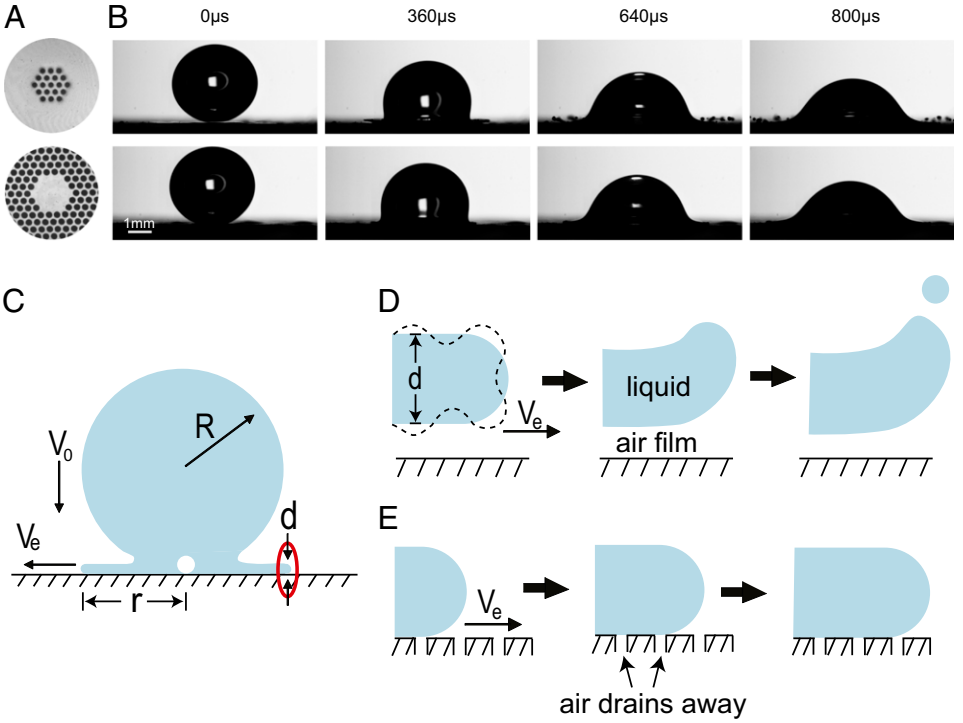

Fig. 2. The air entrapment at the expanding edge causes splashing. (*A*) Images of the two substrates with leaking areas at either the center or the edge. The pores have the diameter 75 ± 5 μm. The top substrate enables a complete drainage of air entrapment at the impact center, and the bottom substrate eliminates air entrapment at the edge. (*B*) Corresponding splashing results on these two substrates, for an ethanol drop with impact velocity $V_0 = 1.92 \pm 0.01$ m/s and diameter 3.5 ± 0.1 mm. Splashing occurs (*Top*) but disappears (*Bottom*), revealing that the air trapped at the expanding edge causes splashing (33). (*C*) A schematic showing the impact geometry and relevant quantities: The impact velocity is V_0, the front expanding velocity is V_e, the expanding radius is r, and the liquid sheet thickness is d. Air is trapped under both the center and the expanding front, but the analysis is focused only at the expanding front (within the red ellipse). (*D*) Cartoon pictures (drawn not to scale) demonstrating the detailed splashing process on a smooth substrate. The ultrathin air film trapped under the liquid initiates the KH instability, as indicated by the dashed curve, which subsequently develops into splashing. (*E*) The corresponding situation on a leaking substrate. No air film exists because air drains away, which consequently eliminates the instability and splashing.

Our model essentially describes a resonance in length scales, $k_m^{-1} = d$, which strongly enhances the KH instability and produces splashing. Because both k_m^{-1} and d can be obtained experimentally, we can quantitatively test this model. In particular, because both k_m^{-1} and d vary with time as the liquid front advances, their match must occur at a specific location, $r = r_0$, where the disturbance from air should be most critical. To explore this critical location, we fabricate various substrates with leaking regions around specific radii, as shown in Fig. 3*A*. The corresponding impact outcomes are demonstrated in Fig. 3*B*: Splashing disappears completely when pores are made around a critical radius, as illustrated in Fig. 3*B*, *Middle*; whereas significant splashing occurs when pores are made at slightly smaller or larger radii, as shown in Fig. 3*B*, *Top* and *Bottom* (Movie S3). Apparently, a critical radius does exist around which the disturbance from air is most critical, and the effective air drainage there completely eliminates splashing. The existence of a critical location agrees well with our resonance picture.

We further verify that exactly at this critical location the resonance condition, $k_m^{-1} = d$, is satisfied. Without any fitting parameter, we directly obtain k_m^{-1} and d from independent measurements and plot them as solid and open symbols, respectively, in Fig. 3*C*. By definition, these two sets of data intersect around r_0 where $k_m^{-1} = d$; in addition, the critical region identified by the leaking substrate in Fig. 3*A* is indicated between the two dashed lines. Clearly the data intersection and the critical region overlap quite nicely, verifying that the critical region for splashing is indeed the resonance location, r_0, predicted by our model. More experiments with different liquids and velocities confirm that the splashing criterion, $k_m^{-1} = d$, is robust and universal (*SI Text*, Table S1, and Fig. S1 *A* and *B*). This criterion also satisfactorily explains the empirical relation observed in the previous experiment (15). We further clarify that although the surface tension dominates viscosity in stabilizing the system, the liquid viscosity does play a role in the model, through its strong influence on V_e and d (15, 19).

More generally, the capability of identifying r_0 with our model enables the quantitative prediction of the precise location, where splashing should first appear, on any smooth substrate. From the experiments on leaking substrates, we have illustrated that draining air around r_0 can either completely eliminate or significantly reduce splashing. Correspondingly, on a smooth substrate without any pores and leakage, the air trapped at r_0 will initiate strong instability and lead to the onset of splashing. Therefore, we can quantitatively predict the splashing onset location on a smooth substrate, by finding r_0 with the intersection of k_m^{-1} and d curves, as shown in Fig. 3*D*, *Inset*. Separately and independently, we can experimentally measure the location where splashing first appears, r_{onset}, with high-speed photography. The measurements from the experiment, r_{onset}, and predictions from our model, r_0, are directly compared in Fig. 3*D*: Under extensive conditions with different liquids, velocities, and substrates, the agreement between the

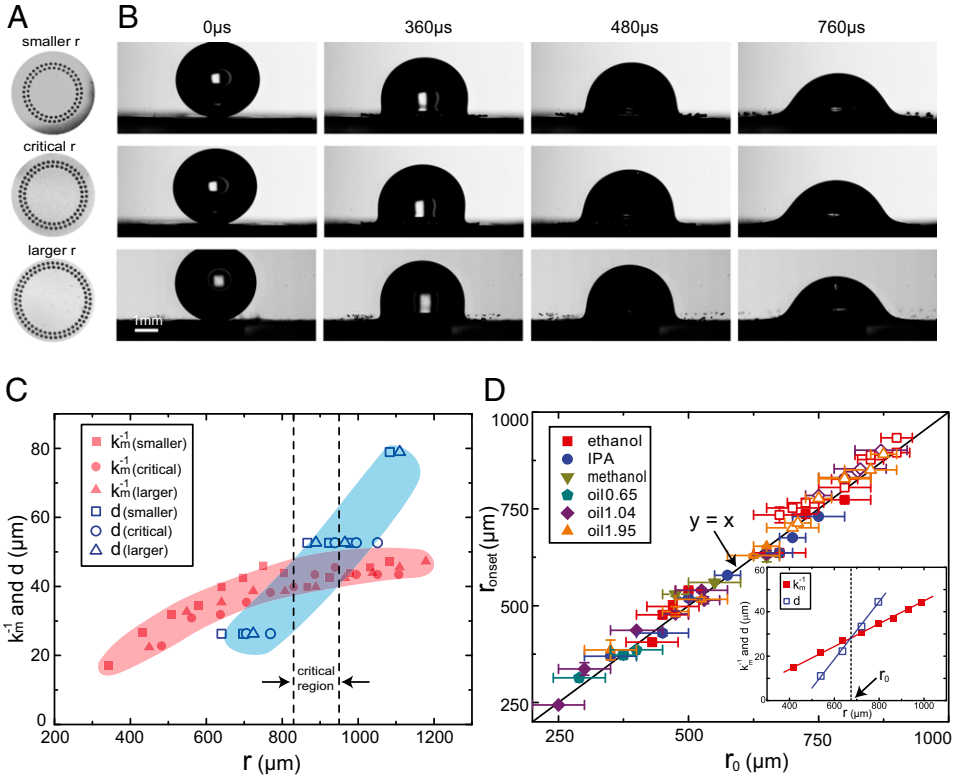

Fig. 3. The match between the instability size and the liquid sheet thickness initiates the splash. (*A*) Three substrates with leaking areas around three different radii: smaller, critical, and larger rs. (*B*) Corresponding splashing outcomes at $V_0 = 1.92$ m/s on these three substrates. Significant splashing appears in *Top* and *Bottom*, but no splashing appears in *Middle*. Apparently a critical radius exists around which the air disturbance is most crucial, and the air drainage there completely eliminates splashing. (*C*) The critical region overlaps with the resonance location r_0, where $k_m^{-1} = d$. We determine r_0 by intersecting k_m^{-1} and d curves from independent measurements (note that d saturates around 50 μm without instability but thickens to 80 μm with instability). The critical region determined by the leaking substrate locates between the two dashed lines. The nice overlap between the curve intersection and the critical region agrees well with our model. (*D*) The splashing onset locations measured from experiments vs. the values predicted by our model on smooth substrates. Shown are various liquids, substrates, and impact velocities; the experimental measurement, r_{onset}, agrees excellently with the model prediction, r_0. The solid and open symbols distinguish the two substrates, glass and optical adhesive NOA81; and different shapes indicate different liquids. (*Inset*) Finding the onset location, r_0, with the model.

experiment and the model is rather outstanding, providing a solid support for our picture of splashing generation.

Discussion

With carefully designed porous substrates, we identify the KH instability initiated within an ultrathin air film as the origin of splashing on smooth surfaces. This picture agrees quantitatively with experimental verifications and illustrates the fundamental mechanism of splashing. However, we clarify that the KH instability provides only a mechanism for the rim formation at the edge, which subsequently takes off; whereas the rupturing of the rim and liquid sheet may involve some other mechanism such as Plateau–Rayleigh instability, which requires further investigation. We also note that our experiments are within the low-viscosity regime, where the surface tension dominates the viscous effect. This provides the basis for the application of KH instability with surface tension only but without viscosity. For the splash of more viscous liquids, the viscous effect should be included and further study is required.

More interestingly, because such air entrapment occurs quite generally for liquid motion on solid substrates, our currently proposed instability may provide a natural mechanism for the common phenomena of liquid–solid wetting during dynamic motions: The growth of the instability within the ultrathin air film may cause the initial touch between liquid and solid, which subsequently develops into the complete wetting. Further study along this direction may illustrate the ubiquitous dynamic-wetting process and make a significant impact on the coating industry. This mechanism could also be crucial for impacts on superhydrophobic surfaces (3, 4, 11, 12), where the air entrapment constantly occurs. The extension of KH instability to the condition of an ultrathin air film further uncovers an interesting direction for this classical instability analysis.

ACKNOWLEDGMENTS. We thank Michael Brenner, Hau Yung Lo, Qi Ouyang, Chu Zhang, and Bo Zheng for great discussion and help. This project is supported by the Hong Kong General Research Fund (GRF) Grants CUHK404211 and CUHK404912 and by The Chinese University of Hong Kong direct Grant 4053081.

1. Worthington AM (1876) On the forms assumed by drops of liquids falling vertically on a horizontal plate. *Proc R Soc Lond* 25(171):261–272.
2. Bergeron V, Bonn D, Martin JY, Vovelle L (2000) Controlling droplet deposition with polymer additives. *Nature* 405(6788):772–775.
3. Richard D, Clanet C, Quéré D (2002) Contact time of a bouncing drop. *Nature* 417(6891):811.
4. Duez C, Ybert C, Clanet C, Bocquet L (2007) Making a splash with water repellency. *Nat Phys* 3(2):180–183.
5. Schroll RD, Josserand C, Zaleski S, Zhang WW (2010) Impact of a viscous liquid drop. *Phys Rev Lett* 104(3):034504.
6. Driscoll MM, Stevens CS, Nagel SR (2010) Thin film formation during splashing of viscous liquids. *Phys Rev E* 82(3):036302.
7. Tsai PA, van der Veen RCA, van de Raa M, Lohse D (2010) How micropatterns and air pressure affect splashing on surfaces. *Langmuir* 26(20):16090–16095.
8. Tsai PA, Hendrix MHW, Dijkstra RRM, Shui L, Lohse D (2011) Microscopic structure influencing macroscopic splash at highWeber number. *Soft Matter* 7(24):11325–11333.
9. Tran AT, et al. (2013) Droplet impact on superheated micro-structured surfaces. *Soft Matter* 9(12):3272–3282.
10. Latka A, Strandburg-Peshkin A, Driscoll MM, Stevens CS, Nagel SR (2012) Creation of prompt and thin-sheet splashing by varying surface roughness or increasing air pressure. *Phys Rev Lett* 109(5):054501.
11. Bird JC, Dhiman R, Kwon H-M, Varanasi KK (2013) Reducing the contact time of a bouncing drop. *Nature* 503(7476):385–388.
12. Liu Y, et al. (2014) Pancake bouncing on superhydrophobic surfaces. *Nat Phys* 10:515–519.
13. Mundo C, Sommerfeld M, Tropea C (1995) Droplet-wall collisions: Experimental studies of the deformation and breakup process. *Int J Multiph Flow* 21(2):151–173.
14. Josserand C, Zaleski S (2003) Droplet splashing on a thin liquid film. *Phys Fluids* 15(6): 1650–1657.
15. Xu L, Zhang WW, Nagel SR (2005) Drop splashing on a dry smooth surface. *Phys Rev Lett* 94(18):184505.
16. Peters IR, Xu Q, Jaeger HM (2013) Splashing onset in dense suspension droplets. *Phys Rev Lett* 111(2):028301.
17. Stevens CS (2014) Scaling of the splash threshold for low-viscosity fluids. *Europhys Lett* 106(2):24001.
18. Riboux G, Gordillo JM (2014) Experiments of drops impacting a smooth solid surface: A model of the critical impact speed for drop splashing. *Phys Rev Lett* 113(2):024507.
19. Xu L (2007) Liquid drop splashing on smooth, rough, and textured surfaces. *Phys Rev E Stat Nonlin Soft Matter Phys* 75(5 Pt 2):056316.
20. Xu L (2010) Instability development of a viscous liquid drop impacting a smooth substrate. *Phys Rev E Stat Nonlin Soft Matter Phys* 82(2 Pt 2):025303.
21. Chandra S, Avedisian C (1991) On the collision of a droplet with a solid surface. *Proc Math Phys Sci* 432(1884):13–41.
22. Thoroddsen ST, Etoh TG, Takehara K (2003) Air entrapment under an impacting drop. *J Fluid Mech* 478:125–134.
23. Thoroddsen ST, Etoh TG, Takehara K, Ootsuka N, Hatsukih Y (2005) The air bubble entrapped under a drop impacting on a solid surface. *J Fluid Mech* 545:203–212.
24. Mandre S, Mani M, Brenner MP (2009) Precursors to splashing of liquid droplets on a solid surface. *Phys Rev Lett* 102(13):134502.
25. Mani M, Mandre SS, Brenner MP (2010) Events before droplet splashing on a solid surface. *J Fluid Mech* 647:163–185.
26. van der Veen RCA, Tran T, Lohse D, Sun C (2012) Direct measurements of air layer profiles under impacting droplets using high-speed color interferometry. *Phys Rev E* 85(2):026315.
27. Tran T, Staat HJJ, Prosperetti A, Sun C, Lohse D (2012) Drop impact on superheated surfaces. *Phys Rev Lett* 108(3):036101.
28. de Ruiter J, Oh JM, van den Ende D, Mugele F (2012) Dynamics of collapse of air films in drop impact. *Phys Rev Lett* 108(7):074505.
29. Liu Y, Tan P, Xu L (2013) Compressible air entrapment in high-speed drop impacts on solid surfaces. *J Fluid Mech* 716:R9.
30. de Ruiter J, Lagraauw R, van den Ende D, Mugele F (2015) Wettability-independent bouncing on flat surfaces mediated by thin air films. *Nature Physics* 11(1):48–53.
31. Lee JS, Weon BM, Je JH, Fezzaa K (2012) How does an air film evolve into a bubble during drop impact? *Phys Rev Lett* 109(20):204501.
32. Driscoll MM, Nagel SR (2011) Ultrafast interference imaging of air in splashing dynamics. *Phys Rev Lett* 107(15):154502.
33. Kolinski JM, et al. (2012) Skating on a film of air: Drops impacting on a surface. *Phys Rev Lett* 108(7):074503.
34. Kolinski JM, Mahadevan L, Rubinstein SM (2014) Lift-off instability during the impact of a drop on a solid surface. *Phys Rev Lett* 112(13):134501.
35. Allen RF (1975) The role of surface tension in splashing. *J Colloid Interface Sci* 51(2): 350–351.
36. Yoon S, Jepsen R, Nissen M, OHern T (2007) Experimental investigation on splashing and nonlinear fingerlike instability of large water drops. *J Fluids Structures* 23(1): 101–115.
37. De Gennes PG (2002) On fluid/wall slippage. *Langmuir* 18(9):3413–3414.
38. Miles JW (1957) On the generation of surface waves by shear flows. *J Fluid Mech* 3:185–204.
39. Lamb H (1945) *Hydrodynamics* (Dover, New York), 6th Ed.

Supporting Information

Liu et al. 10.1073/pnas.1417718112

SI Text

Materials and Methods

We use multiple low-surface-tension and low-viscosity liquids to perform our experiments, as listed in Table S1. The low surface tension makes splashing occur easily and reproducibly, and the low viscosity guarantees that we are not in the high-viscosity regime where a different type of splash occurs (1). The experimental results from different liquids are all consistent with each other, indicating the robustness of our findings.

We make the substrates with the optical lithography technique. First, we spin coat a thin layer of UV-epoxy (SU8-2025; MicroChem) onto a clean silicon wafer and then cover the wafer with a mask of predesigned pattern and expose it under UV light. After development, arrays of holes are made on the epoxy layer. Then we fill liquid polydimethylsiloxane (PDMS) into this structure and solidify it, achieving a PDMS layer with circular pillars. At the end we fill optical adhesive (NOA81; Norland Products) into this PDMS structure and solidify it, obtaining transparent substrates of NOA81 with arrays of holes. The thicknesses of the substrates are typically 50 μm and the diameters of holes are 75 ± 5 μm. Typical examples are shown in Figs. 1–3 in the main text.

1. Xu L (2010) Instability development of a viscous liquid drop impacting a smooth substrate. *Phys Rev E Stat Nonlin Soft Matter Phys* 82(2 Pt 2):025303.

The Match Between k_m^{-1} and d for Various Situations

As demonstrated in Fig. 3*C* in the main text, we have experimentally verified that the critical region for splashing initiation is indeed at the location where the instability size, k_m^{-1}, matches the liquid tip thickness, d. To confirm its general robustness, here we show more experiments with different liquids and velocities. In Fig. S1*A* we show the results of an ethanol drop impacting on the optical adhesive NOA81 substrates with $V_0 = 2.16$ m/s. The data for two substrates are shown: One has pores around the critical radius and the other is completely smooth without pores. We note that for the critical substrate, splashing is significantly eliminated (around 80%) but not completely eliminated; whereas for pores made at other locations the splashing reduction is far less significant. In Fig. S1*B* we use a different liquid, oil-1.04, and eliminate splashing completely by making pores around the critical radius. All data demonstrate that the critical region for splashing overlaps with the region around r_0, where k_m^{-1} matches d. Moreover, we also illustrate the exact approach of how to find r_0 values on a smooth substrate. With our model, we can predict the splash onset location, r_0, by intersecting k_m^{-1} and d curves, as shown in Fig. S1 *C* and *D*: Each panel determines one particular r_0 value used in Fig. 3*D* in the main text.

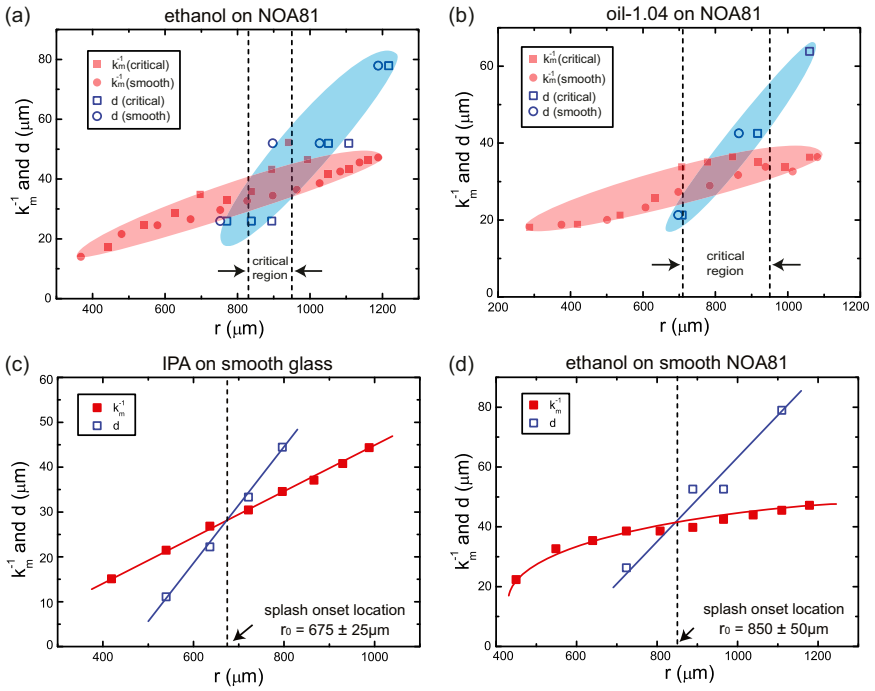

Fig. S1. The match between k_m^{-1} and d for various liquids, substrates, and impact velocities. (*A*) An ethanol drop impacting on NOA81 substrates with $V_0 = 2.16$ m/s. The data for two substrates are shown: One has pores around the critical radius and the other is completely smooth without pores. (*B*) An oil-1.04 drop impacting on NOA81 substrates with $V_0 = 1.92$ m/s. Again the data for two similar substrates as in *A* are shown. (*C*) An isopropyl alcohol (IPA) drop impacting on a smooth glass substrate with $V_0 = 2.04$ m/s. From the cross of the two curves, we can determine the splash onset location with our model, which gives one value of r_0 for Fig. 3*D* in the main text. (*D*) An ethanol drop impacting on a smooth NOA81 substrate with $V_0 = 1.92$ m/s. Again we can determine one value of r_0 for this impact condition.

Table S1. Material properties of different liquids

Liquid	ρ, kg/m^3	σ, mN/m	μ, mPa·s	Drop diameter, mm
Methanol	791	22.1	0.61 ± 0.02	3.5 ± 0.1
Ethanol	789	22.6	1.15 ± 0.02	3.5 ± 0.1
IPA	786	21.7	2.07 ± 0.02	3.5 ± 0.1
Oil-0.65	760	15.9	0.65 ± 0.02	3.0 ± 0.1
Oil-1.04	816	17.4	1.04 ± 0.02	3.0 ± 0.1
Oil-1.95	873	18.7	1.95 ± 0.02	3.0 ± 0.1

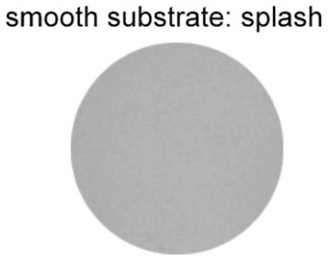

Movie S1. Significant splash occurs on the smooth substrate, no splash appears on the leaking substrate, and splash reappears on patterned but nonleaking substrate. $V_0 = 1.92$ m/s.

Movie S1

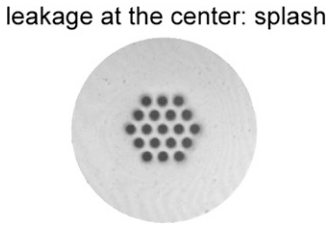

Movie S2. Air leakage at the center still leads to splash, whereas air leakage at the edge eliminates splash. V_0 = 1.92 m/s.

Movie S2

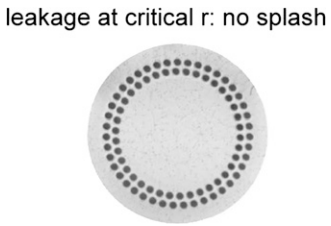

Movie S3. Air leakage at the critical radius r_0 eliminates splash completely, but air leakage at a smaller or a larger radius still leads to splash. V_0 = 1.92 m/s.

Movie S3